Time Domain Diffuse Correlation Spectroscopy for Detecting Human Brain Function: Optimize System on Real Experimental Conditions by Simulation Method

Lina Qiu, Tingzhen Zhang, Wen Huang, Weiting Sun, Xiaoyin Wu, Huiwen Sun, Fang Lin, and Jun Li

***Abstract*—In order to achieve high-sensitivity time-domain diffuse correlation spectroscopy (TD-DCS) measurement of functional changes in cerebral blood flow, this study applied simulation methods to optimize the TD-DCS system under real experimental conditions (including the consideration of the effects of finite coherence length L_C and non-ideal instrument response function IRF). Under a real experimental condition where the incident power is 75 mW, the source-detector distance is 1.0 cm, and the full width at half maxima of the IRF is 160 ps, we used simulation experiments to investigate the relationship between the contrast of the intensity autocorrelation function (g_2) in two brain functional states (i.e., baseline and activation) and TD-DCS system parameters (including L_C, IRF, source-detector distance, gate opening time and gate width).Our simulation results show that both longer L_C and longer integration time are beneficial to a more sensitive detection. With a fixed L_C and integration time, the optimal parameters of gate opening time is 800 ps (relative to the peak time of IRF), and gate width is equal to or larger than 800 ps. This study may be useful for guiding the sensitive measurement of human brain functions (e.g., changes in cerebral blood flow) using the TD-DCS technology.**

***Index Terms*—Time domain diffuse correlation spectroscopy, simulation, system optimization, brain functional detection, sensitivity.**

Manuscript received April 12, 2021; revised May 28, 2021; accepted June 11, 2021. Date of publication June 15, 2021; date of current version July 5, 2021. This work was supported by the Guangzhou Science and Technology Plan Project Key Field R & D Project under Grant 202007030005, in part by the Natural National Science Foundation of China (NSFC) under Grant 81771876, in part by the Guangdong Basic and Applied Basic Research Foundation under Grant 2019A1515110388, in part by Guangdong Provincial Key Laboratory of Optical Information Materials and Technology under Grant 2017B030301007, in part by Guangdong Science and Technology Program under Grant 2017A010101023, in part by Special Funds for the Cultivation of Guangdong College Students' Scientifi c and Technological Innovation ('Climbing Program' Special Funds) under Grant pdjh2020b0155, and in part by Science and Technology Program of Guangzhou under Grant 2019050001. *(Lina Qiu and Tingzhen Zhang authors contributed equally.) (Corresponding author: Jun Li.)*

Lina Qiu is with the School of Software, South China Normal University, Guangzhou, Guangdong 510631, China (e-mail: lina.qiu@scnu.edu.cn).

Tingzhen Zhang, Wen Huang, Weiting Sun, Xiaoyin Wu, Huiwen Sun, and Fang Lin are with the South China Academy of Advanced Optoelectronics, South China Normal University, Guangzhou, Guangdong 510631, China (e-mail: tingzhen.zhang@coer-scnu.org; wendy@coer-scnu.org; weiting.sun@coer-scnu.org; xiaoyin.wu@coer-scnu.org; huiwen.sun@coer-scnu.org; fang.lin@coer-scnu.org).

Jun Li is with the South China Academy of Advanced Optoelectronics, and Key Lab for Behavioral Economic Science and Technology, South China Normal University, Guangzhou, Guangdong 510631, China (e-mail: jun.li@coer-scnu.org).

Digital Object Identifier 10.1109/JPHOT.2021.3089635

I. Introduction

DIFFUSE correlation spectroscopy (DCS) is an optical technique that was originally used to measure the dynamic properties of scattering media, such as latex and colloidal suspensions [1]–[7]. In DCS, a laser beam with a long coherence length illuminates a liquid turbid sample. The incident photons are multiply scattered inside the sample, and part of which emerge from the surface of the sample. The emitted photons with different path lengths constructively or destructively interfere with each other, thus forming a speckle pattern on the surface. Since the scattering particles in the sample are moving (e.g., Brownian motion), the speckles are fluctuating. DCS measures the temporal intensity autocorrelation function (g_2) of a single speckle to characterize the dynamic properties of the sample. The g_2 is a decay curve with respect to the lag time τ, reflecting the dynamical properties of the sample [2]. In recent years, DCS has been successfully used for measuring the blood flow (e.g., blood flow index, BFi) including the cerebral blood flow (CBF), and it is becoming an important optical imaging modality for studying human tissues and brain. To date, the biomedical applications of DCS include but are not limited to characterizing tumor micro-vessels, monitoring chemotherapy [3], [7] and monitoring or estimating cerebral blood flow and oxygenation in human brain [4], [6].

The traditional DCS technique typically utilizes a continuous wave (CW) laser with a coherence length longer than the spread of path length distribution of the detected light to ensure that light from different paths can interfere fully at the detector [5]. Since the CW laser is used as the light source, the traditional DCS is also termed as CW-DCS. In CW-DCS, the intensity autocorrelation function is calculated from all detected photons with various path lengths, therefore it is not ready to distinguish the dynamics sampled by different paths. In addition, since the measured autocorrelation function (for 2-3 cm source-detector spacing, typically used in measuring functional activation in human brain) is mainly dominated by

the contribution of the superficial dynamics, the contrast induced by the change in deep dynamics is extremely small, therefore, CW-DCS cannot detect the deep dynamics (e. g., from deep brain cortex) sensitively and effectively. However, in biomedical applications, the hemodynamics in deep tissues (such as the cerebral hemodynamics) is more valuable and informative for the diagnosis and treatment of diseases than the hemodynamics in superficial tissues. One possible way to solve this problem is to use a long source-detector (SD) distance. Extending the SD distance can effectively increase the penetration depth and thus enhance the detection sensitivity to the deep dynamics. However, it is worth noting that while increasing the SD distance, the number of detected photons is also significantly reduced, thereby increasing the noise level of the measured temporal intensity autocorrelation function g_2 [5]. Especially for DCS that uses single-mode fiber with a small core diameter and a low numerical aperture to collect photons, a long SD distance can easily reduce the signal-to-noise ratio (SNR) of the measured g_2. Although increasing the power of the incident laser can also increase the SNR of g_2, it is worth noting that the incident light power density must comply with the human tissue safety criteria of ANSI Z136.3 (2018) - Safe Use of Lasers in Health Care [8]. In other words, when using DCS to measure human tissues (such as human brain), the power of the incident laser cannot be increased arbitrarily and must be carefully controlled within the safety limits. The other possible way to improve the detection sensitivity to deep dynamics is to detect or analyze photons that only pass through deep tissues, which led to the emergence of time-domain (TD) DCS technology, called TD-DCS [9].

TD-DCS combines the merits of traditional DCS and TD detection techniques, allowing simultaneous acquisition for the temporal point-spread function (TPSF) of the light that can quantify the optical properties of tissues and the autocorrelation function that can quantify the BFi. More importantly, TD-DCS can differentiate between short photon paths and long photon paths through the tissue by a time-gated strategy [10] and separate the contribution of different path lengths to g_2, thereby determining the dynamic information from the superficial tissues and the deep tissues. In other words, TD-DCS can provide higher sensitivity detection for deep dynamics. In recent years, TD-DCS technology has developed rapidly, including the proposal of various theoretical models, the verification of simulation and phantom experiments, as well as in vivo measurement of the human arm and head [11]–[17].

TD-DCS uses a pulsed laser with a very limited coherence length, thus the measurement is inevitability affected by the instrument response function (IRF) and laser coherence length (L_C). In order to obtain highly sensitive TD-DCS measurement of deep dynamics, in addition to the above two factors, some other experimental factors (e.g., gate opening time and gate width, SD distance) should be considered in the experimental design and data analysis. Very recently, we have optimized some experimental factors on a realistic head model based on the simulation method, including SD distance and gate opening time and gate width [13]. The results showed that under acceptable input power of light, a high-contrast measurement of deep dynamic changes (e.g., cerebral blood flow caused by functional activation) can be achieved by selecting the optimal combination of SD distance(s) and time gate(s). We found that SD distance of 0-1.5 cm, gate opening time of 700-800 ps, and gate width of 800 ps are optimal options. However, that study has several limitations. For instance, we did not consider the effect of IRF and the finite L_C, which are two key factors that affect the real TD-DCS measurement. Regarding the effect of these two factors on TD-DCS measurement, Cheng et al. have developed an analytical model of time-resolved g_2 containing IRF and L_C factors and applied it to semi-infinite medium [12]. In addition, Colombo et al. [14] took the IRF into account and proposed a model for retrieving the blood flow from the gated intensity autocorrelation function, in which improved the in TD-DCS measurements. However, the above two studies were based on the semi-infinite model, and the effect on more complex heterogeneous media (such as human head) is not yet clear.

Therefore, to obtain a more accurate and sensitive TD-DCS measurement of cerebral blood flow under limited input laser power, we need to consider a more realistic TD-DCS measurement of human cerebral blood flow. In this study, we simulated the real measurement of TD-DCS on a head model based on the previous study [13], and further considered the effect of L_C and IRF. In this simulation experiment, we studied the effect of IRF, L_C, gate opening time and gate width on the TD-DCS intensity autocorrelation function (g_2). For this, we used an optimal SD distance (i.e., SD $=$ 1.0 cm) obtained from our previous study [13] and utilized a mimic IRF and L_C with several possible values for a real TD-DCS system. A Monte Carlo simulation was first performed on the frontal lobe of a realistic human head model to obtain the TPSF of the detected photons, and then the time-resolved (or path length resolved) intensity autocorrelation functions (g_2) for the two brain functional conditions (i.e., baseline and activation) were simulated. Finally, the optimal combination of L_C, gate opening time and gate width were sought to achieve a high-contrast measurement of changes in cerebral blood flow.

II. Methods

A. Theory

The signal recorded in the real DCS measurement is the intensity autocorrelation function g_2 which is related to the electric field autocorrelation function g_1 by the Siegert relation $g_2 = 1 + \beta|g_1|^2$ [18], where β is the intercept of g_2, that is, the value of g_2 at zero lag time. β is a parameter that depends on the experimental setup, including the laser coherence length and stability of the laser, as well as the number of modes in the detection fiber. For an unpolarized light source, if its coherence length is long enough, $\beta = 0.5$ when single-mode fiber is used for photon detection.

For CW-DCS measurements, the autocorrelation function comes from contributions of all possible path lengths of detected photons. Unlike CW-DCS, TD-DCS measurement can use the time-gated strategy to distinguish photons from deep or superficial tissues according to the time when the photons reach

the detector [10]. In the Brownian motion model that can better explain the experimental data measured from tissues in the body including the human brain, the normalized field autocorrelation function within a specific time gate (e.g., $[t_1,\ t_2]$) can be expressed as:

$$g_1\ (\tau, [\,t_1,\ t_2]) = \int_{t_1}^{t_2} P\left(t = \frac{s}{v}\right) \exp\left(-2k^2\mu_s' s D_B \tau\right) dt \tag{1}$$

where τ is the lag time, k is the wave number in the medium, μ_s' is the reduced scattering coefficient, and D_B is the Brownian diffusion coefficient of the scattering particles. $P(t)$ is the fraction of photons with a time-of-flight of s/v within the gate, where s is the propagation path length and v is the speed of light in the medium.

When the experimental system is ideal (e.g., the effect of IRF and L_C can be neglected), the normalized intensity autocorrelation function $g_2(\tau, [\,t_1,\ t_2])$ in the time gate described by $[t_1,\ t_2]$ can be expressed as follows according to the Siegert relation:

$$g_2\ (\tau, [\,t_1,\ t_2]) = 1 + \beta\left(\int_{t_1}^{t_2} g_1(\tau, t)\cdot TPSF(t)\,dt \Big/ \int_{t_1}^{t_2} TPSF(t)\,dt\right)^2 \tag{2}$$

where TPSF is the temporal point-spread function, which can be obtained from real experiment collection or numerical simulation.

In the real measurement using the TD system, due to the effect of IRF, the path length of the detected photons at time t within the gate is no longer $v \cdot t$, and most of them may be shorter than $v \cdot t$. Therefore, the role of IRF in real TD-DCS measurement cannot be ignored. When the coherence length of the laser is infinite or much longer than the photon path length, the effect of the coherence length on g_2 can be ignored. In this case, the normalized intensity autocorrelation function g_2 in the time gate $[t_1,\ t_2]$ under the effect of IRF can be calculated as [12]:

$$g_2\ (\tau, [\,t_1,\ t_2]) = 1 + \beta\left(\int_{t_1}^{t_2}\int_{0}^{t} g_1(t,\tau)\cdot IRF(t-t_0) \cdot TPSF(t_0)\,dt_0 dt \Big/ \int_{t_1}^{t_2}\int_{0}^{t} IRF(t-t_0)\cdot TPSF(t_0)\,dt_0 dt\right)^2 \tag{3}$$

However, the coherence length L_C of the laser cannot be infinitely long, especially in the TD-DCS system, the pulse width of the light source is relatively narrow. Due to the limitation of the uncertainty principle, the influence of L_C on the measurement result (such as g_2) cannot be ignored. Therefore, when considering the influence of IRF and L_C on TD-DCS measurement at the same time, $g_2(\tau, [\,t_1,\ t_2])$ can be expressed as:

$$g_2(\tau, [\,t_1,\ t_2]) = 1 + \beta\left(\frac{1}{\gamma^2}\right)\cdot \int_{t=t_1}^{t=t_2} \int_{t_0=0}^{t_0=t} IRF(t-t_0) TPSF(t_0)\, g_1(t_0,\tau)\, dt_0 \int_{t'=t_1}^{t'=t_2} \int_{t_0=0_1}^{t_0=t'} IRF(t'-t_0)\, TPSF(t_0)\, g_1(t_0,\tau)\, dt_0 \cdot exp\left[-2\left(\frac{v(t-t')}{L_c}\right)^2\right] dt' dt \tag{4}$$

where $\gamma = \int_{t_1}^{t_2}\int_{0}^{t} IRF(t-t_0)TPSF(t_0)dt_0 dt$ is a normalization factor. When IRF is the Dirac Delta function $\delta(t)$ and L_C is much longer than maximal difference between path lengths, Equation (4) can be simplified to Equation (2).

TABLE I.
OPTICAL PROPERTIES AT 830 NM USED IN MC SIMULATIONS ON THE ATLAS-BASED HEAD MODEL

Tissues	$\mu_a(mm^{-1})$	$\mu_s'(mm^{-1})$
Skin and Skull	0.0191	0.66
Cerebral Spinal Fluid	0.0026	0.01
Gray Matter	0.0186	1.11
White Matter	0.0186	1.11

B. Simulation Experiments

In this study, we used a simulation method to simulate the real measurement of dynamic changes in the deep (cortical) layer of the human brain by TD-DCS on the human head model. The experiment mainly measured the frontal cortex area.

In the simulation experiment, we first used a Mesh-based Monte Carlo (MMC) method to simulate the propagation of photons in the human brain on a realistic human head model. MMC is a Monte Carlo method proposed by Fang et al., which can effectively simulate light propagation inside structures with complex boundaries [19]. The human head model used in the simulation is Colin27 Brain Atlas FEM Mesh (Version 2) created based on the Colin27 brain model [20]. This human head model consists of five different tissues: skin and skull (SS), cerebral spinal fluid (CSF), gray matter (GM), white matter (WM) and ventricles. Since Near infrared light cannot reach the ventricles, we only considered SS, CSF, GM and WM in our simulations. The average thickness of SS, CSF and GM tissues are 14.5 mm, 2 mm and 4 mm, respectively. The optical properties (including absorbing coefficient μ_a and reduced scattering coefficient μ_s') of these four tissues at the illumination wavelength of 830 nm are shown in Table I [21].

During the MMC simulation, a beam of light was injected perpendicularly to the surface of on the frontal lobe of the head model, and the positions of the optical probes are shown in Fig. 1. The SD distance was set to 1.0 cm, which is not only one of the optimal SD distance for TD-DCS to measure the cortical dynamic changes found in our previous study [13], but also a common distance in vivo TD near-infrared spectroscopy measurements [22]. The number of incident photons is about 1.4×10^9. From the MMC simulation, the surviving weight and partial pathlength of each emitted photon can be obtained, and then the TPSF a given SD distance of 1.0 cm can be calculated, which is the result of calculation when the system is ideal (that is, the effect of IRF is not considered). However, in the real measurement using TD system, the role of IRF cannot be ignored. In the commonly used TD-DCS system, the full width at half maxima (FWHM) of the IRF in is about 100-300 ps [14],

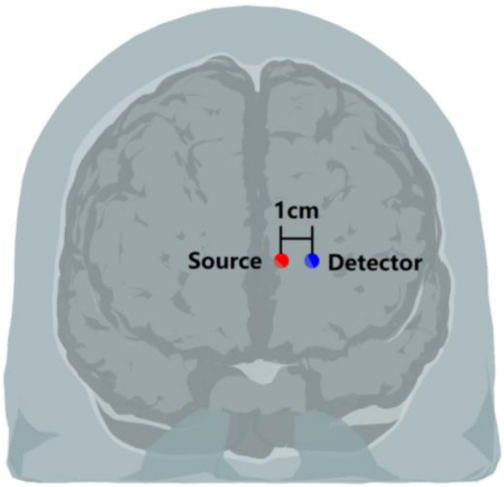

Fig. 1. Locations of the optical probes on the frontal lobe of the head model. The red and blue dots represent the source and detector, respectively. The light illuminates perpendicular to the surface of the head. The SD distance is 1.0 cm.

[23]. In order to simulate the real TD-DCS measurement more realistically, we synthesized a right-tailed IRF with a FWHM of about 160 ps and a peak time of 2000 ps, as shown in the red curve in Fig. 2. The long right tail is a characteristic of the single-photon avalanche diode commonly used in TD systems [14], [24]. The TPSF obtained from MMC simulation and the diffuse reflectance after convolution of TPSF and IRF are also displayed in Fig. 2.

In this study, we evaluated the sensitivity of TD-DCS to measure cortical dynamic changes (e.g., changes in cerebral blood flow) by simulating the g_2 signal of the brain under two functional conditions (i.e., baseline and activation), aiming to optimize some experimental parameters to obtain high-sensitivity measurement, including the gate opening time (t_0) and gate width (T) under fixed system parameters such as incident power of light, L_C, IRF and core diameter and numerical aperture (NA) of the single-mode detection fiber. The Brownian diffusion coefficients (D_B) of the four brain tissues of SS, CSF, GM and WM under the baseline state were respectively assumed to be $1 \times 10^{-6} mm^2/s$, 0, $6 \times 10^{-6} mm^2/s$ and $2 \times 10^{-6} mm^2/s$, and their D_B under the activation state were assumed to be $1 \times 10^{-6} mm^2/s$, 0, $9 \times 10^{-6} mm^2/s$ and $3 \times 10^{-6} mm^2/s$ [9], [25].

In the simulated experiment, a pulsed laser with an average power of 75 mW at 830 nm was injected into the head model with a repetition rate of 100 MHz. For the photon detectors (e.g., avalanche photodiodes, APD), a single-mode fiber with a core diameter of 6.9 μm and NA of 0.14 was used, and the quantum efficiency was set to 40%. Two time-resolutions (or integration time) of 5 s and 10 s were set for measurement, which are marginally acceptable in brain functional study. Since the number of photons detected within the selected time gate for each incident pulse can be calculated from the MMC simulation, it is possible to simulate the g_2 signals of the brain under baseline and activation conditions by generating a photon sequence with a known count rate and correlation between photons. The intercept of g_2 ($\tau = 0$) is randomly generated in the simulation.

We used the signal-to-noise ratio (SNR) defined as $SNR = S/N$ to evaluate the measurement sensitivity of TD-DCS to CBF change between the baseline and activation conditions. The S is the maximal difference of g_2 (i.e., $\Delta g_2\ (\tau = \tau_m)$) between the baseline and activation condition, where τ_m is the lag time when the difference in g_2 between the baseline and activation was maximal. The N is the noise level of g_2 at $\tau = \tau_m$ for the baseline and activation, e.g., $N = \sqrt{STD^2_{baseline} + STD^2_{stimulation}}$, where STD is the standard deviation of g_2 at $\tau = \tau_m$. The higher the SNR value obtained, the greater the contrast of g_2 measured in the baseline and activation condition, indicating that TD-DCS is more sensitive to the measurement of cerebral blood flow changes.

III. Results

From the MMC simulation, we can directly obtain the path length distributions and corresponding weights of all photons received by the detector, and then calculate the TPSF for each incident photon, as shown in the black curve in Fig. 2. Compared with the TPSF curve, the time-resolved diffuse reflectance (blue curve in Fig. 2) obtained after convolution of TPSF and IRF (red curve in Fig. 2) has a delay in the peak time and a wider shape. Early arriving photons usually have shorter propagation paths, while late photons have longer propagation paths. Therefore, most early photons only carry information from superficial tissues, while later photons may carry information from both superficial and deep tissues (such as brain). In a TD system, different time gates can be selected to distinguish between long optical paths and short optical paths. For TD-DCS, the intensity autocorrelation function g_2 measured in different time gates may reflect dynamics of tissues at different depths. For example, g_2 with longer paths (or in a later gate) is more sensitive to the deeper dynamics. However, the number of photons detected with longer paths is generally small, resulting in a relatively high noise level on the measured g_2. Therefore, in a real TD-DCS measurement with a limited incident light power, selecting an appropriate time gate (i.e., gate opening time t_0 and gate width T) is critical to achieve a sensitive TD-DCS measurement of cerebral blood flow.

In addition to the time gate, IRF and L_C also affect the contrast of g_2 between baseline and activation conditions, even without any photon noise, as shown in Fig. 3. In the case of no IRF effect and infinite L_C (Fig. 3(a)), the maximal difference of g_2 between the baseline and activation is 0.0296. In the case of no IRF effect but limited L_C (e.g., L_C= 10 cm), the maximal difference is 0.0196, as shown in Fig. 3(b). When considering IRF and infinite L_C (Fig. 3(c)), the maximal difference is 0.0118. When considering IRF and limited L_C (e.g., L_C= 10 cm), the maximal difference is 0.0079, as shown in Fig. 3(d). Therefore, any factor of IRF or finite L_C can lead to a decrease in the measurement contrast, which may become much smaller in the presence of both IRF and finite L_C effects.

It is rather straightforward to consider that using a narrow IRF photon detection system and a long L_C pulsed laser to

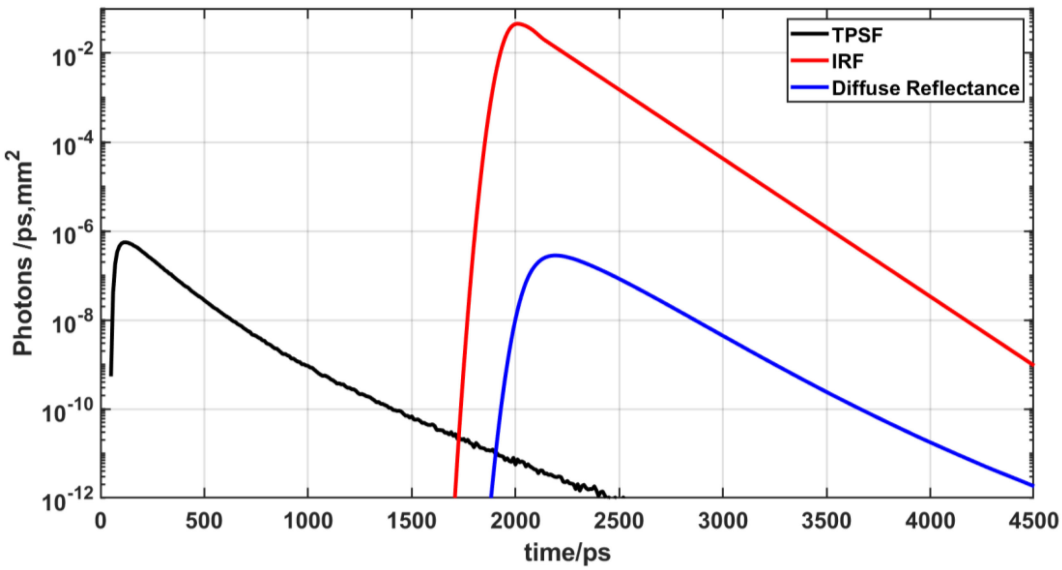

Fig. 2. The TPSF (black curve) obtained by MMC simulation at SD = 1.0 cm, the right tailed IRF (red curve) with FWHM of 160 ps, and a peak time of 2000 ps, and the diffuse reflectance (blue curve) after convolution of TPSF and IRF.

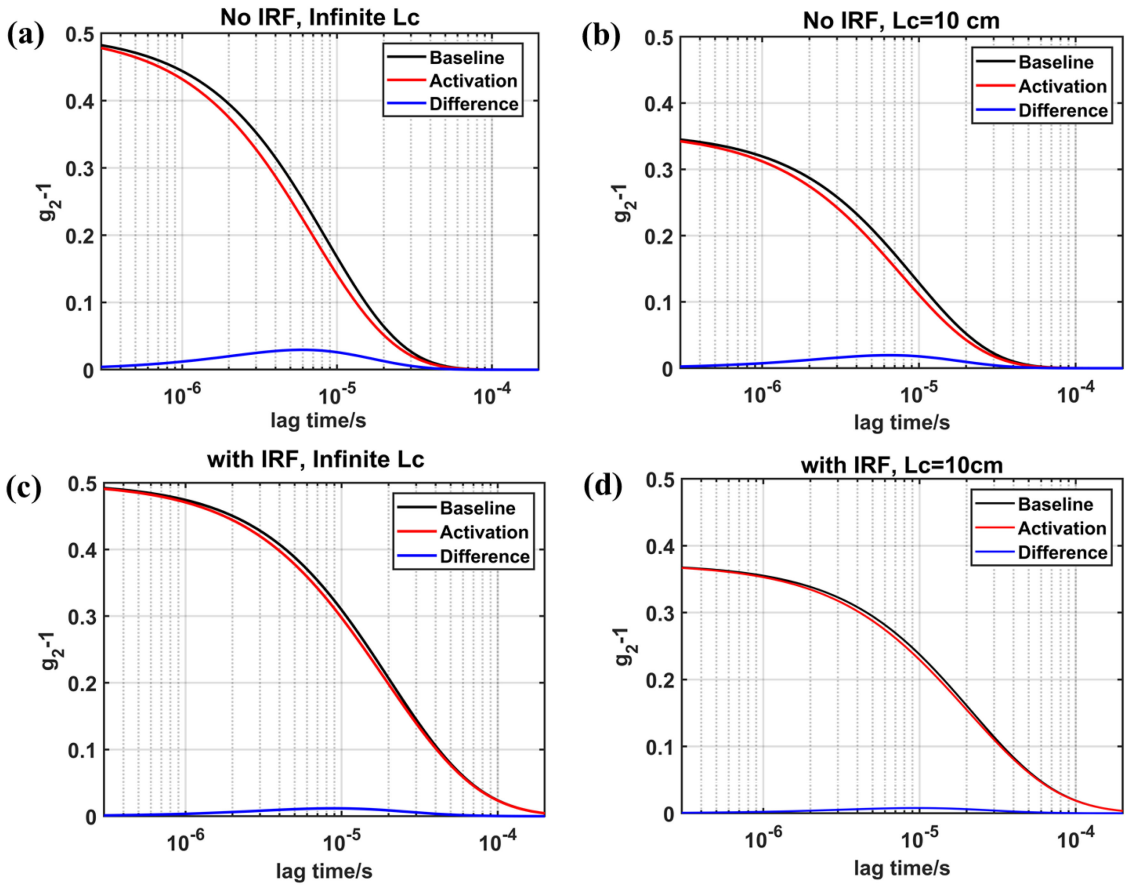

Fig. 3 The intensity autocorrelation function g_2 with no IRF effect and infinite L_C (a); g_2 with no IRF effect but with L_C= 10 cm (b); g_2 with IRF effect and infinite L_C (c); g_2 with IRF effect and L_C= 10 cm (d). Here, the gate opening time is t_0= 1000 ps and the gate width is T = 1000 ps. In the absence of IRF effect, t_0 is relative to time zero, and in the case of IRF effect, t_0 is relative to the peak time of the IRF.

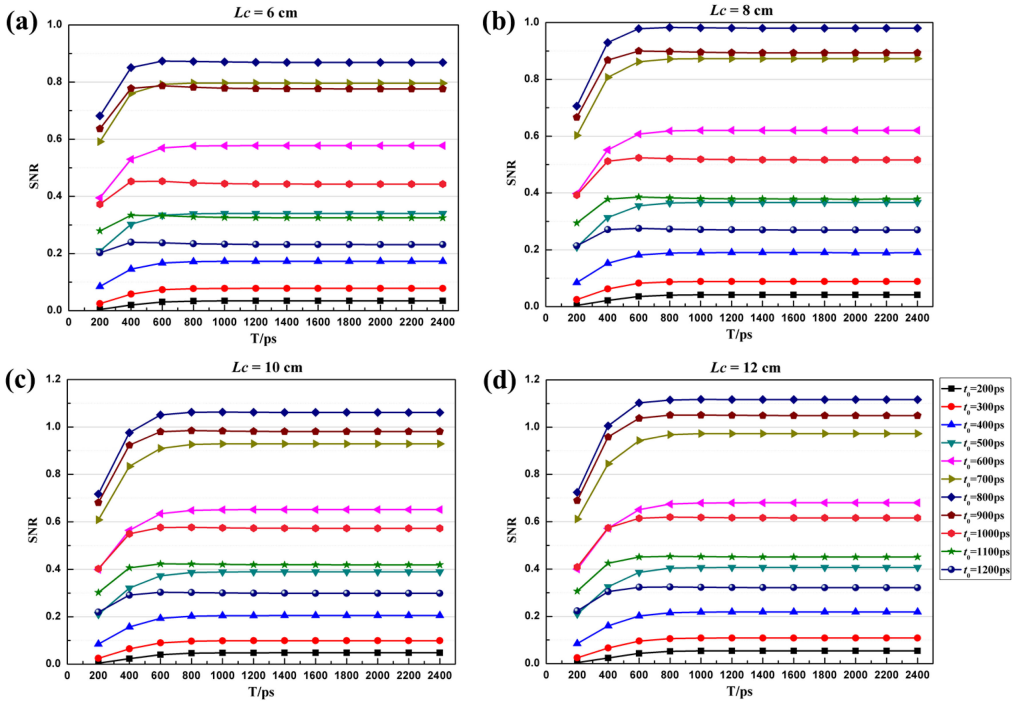

Fig. 4 SNR calculated with different gate opening time t_0 and gate width T for 5 s integration time when L_C= 6 cm (a), L_C= 8 cm (b), L_C= 10 cm (c) and L_C= 12 cm (d).

improve the measurement contrast in TD-DCS. However, the fact is that any pulsed laser has a limited L_C due to Heisenberg's uncertainty principle (i.e., $\Delta\nu \geq 1/4\pi\Delta t$, $\Delta\nu$ is frequency line-width of the laser light, Δt is the pulse width). Since the coherence length L_C is proportional to the inverse of $\Delta\nu$ (e.g., $L_C = 2\ln(2) \cdot (c/n) \cdot (1/\pi \cdot \nu)$ for a Gaussian spectrum), the narrower the pulse width is, the shorter the coherence length L_C. On the other hand, the IRF comes from the combination of laser pulse width and the response time of the photon detection devices. Therefore, the width of the IRF cannot be narrower than the width of the laser pulse. In other words, in an actual TD-DCS system, the upper limit of the coherence length is limited by the width of IRF. For example, we assumed in this simulation that the FWHM of the IRF is 160 ps, then the L_C must be shorter than 19.0 cm (in the medium with a refractive index of $n = 1.4$). In practice, the L_C is usually well below the upper limit.

The inability to obtain a laser light source with a long L_C and a narrow pulse at the same time is a common problem faced by any TD-DCS system. L_C that is not long enough and IRF that is too wide both will cause a decrease in the contrast of g_2 between baseline and stimulus conditions, thereby reducing the sensitivity of TD-DCS to cerebral blood flow measurement. In the actual situation where L_C is limited and IRF is not ideal (such as a Delta function), this problem can be improved by optimizing measurement parameters such as gate opening time t_0 and gate width T.

On the condition of 75 mw incident power and SD = 1.0 cm, we performed simulation of g_2 with L_C= 6-12 cm (at an interval of 2 cm) and the integration time (or time resolution of g_2) of 5 s and 10 s, respectively. Then the SNR corresponding to different gate opening time t_0 (relative to the peak time of the IRF) and gate width T were calculated and plotted, as shown in Fig. 4(integration time = 5 s) and Fig. 5(integration time = 10 s). For any fixed gate (i.e., fixed opening time t_0 and gate width T), the SNR increased with the increase of L_C and the integration time. The larger SNR values occurred mostly at t_0= 800 ps and $T\geq$800 ps. Most of these SNR values in these time gates (i.e., t_0= 800 ps and $T\geq$800 ps) are larger than 1, except for the cases of $L_C\leq$8.0 cm (e.g., 6.0 and 8.0 cm) when the integration time = 5 s, as shown in Fig. 4(a)-(b). When $L_C\leq$8.0 cm, there is no SNR larger than 1 for integration time = 5 s, indicating that when the coherence length is less than 8.0 cm, it is impossible to detect changes in cerebral blood flow in human brain with a temporal resolution less than 5 s. The largest value of SNR in our simulation is 1.580, occurring at integration time = 10 s, L_C= 12 cm, t_0= 800 ps and T = 1000 ps, as shown in Fig. 5(d). In addition, the SNR value of the integration time of 10 s is always larger than the integration time of 5 s under each combination of t_0, T and L_C.

IV. Discussions

In our previous work [13], we performed a similar simulation study using the same head model but neglecting the IRF and L_C effects, we found that using the parameter combination such as SD = 0-1.5 cm, t_0= 700-800 ps and $T\geq$800 ps could lead to higher TD-DCS measurement contrast on the cerebral blood flow. The result of the present study is that using SD = 1.0 cm, t_0= 800 ps and $T\geq$800 ps can result in a higher SNR (see Fig. 4 and Fig. 5), which is quite similar to the previous finding. However, the obtained SNR values are much lower than the SNR values without the effects of IRF and L_C. This

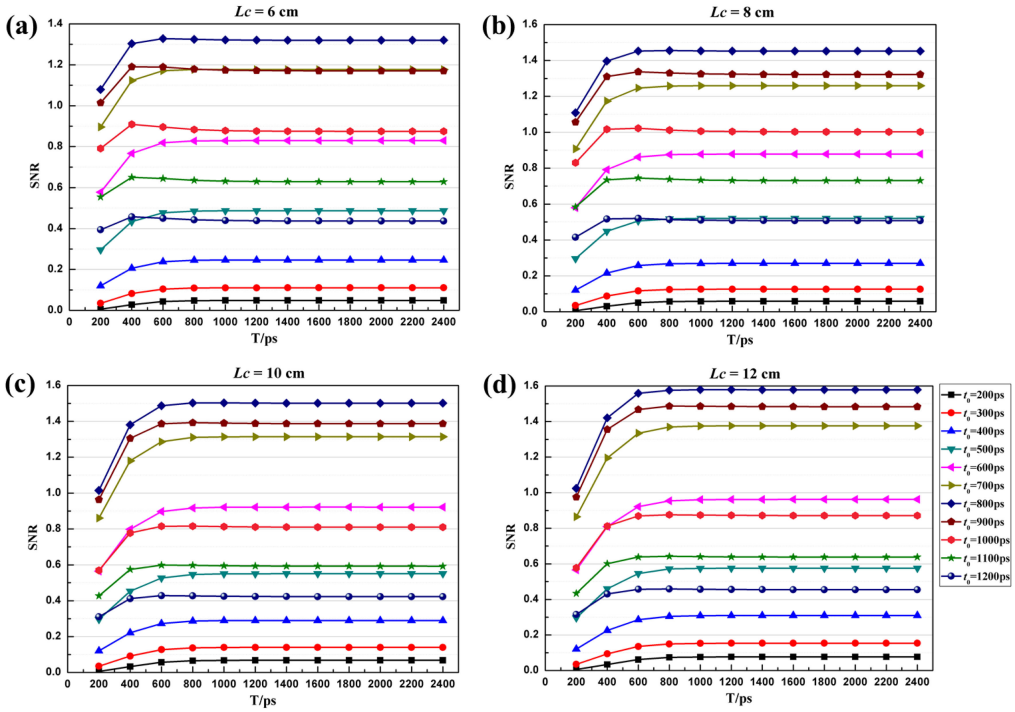

Fig. 5 SNR calculated with different gate opening time t_0 and gate width T for 10 s integration time when L_C= 6 cm (a), L_C= 8 cm (b), L_C= 10 cm (c) and L_C= 12 cm (d).

demonstrates again that IRF and L_C have significantly adverse influences on the contrast of TD-DCS measurement even in the absence of photon noise (see Fig. 3). Considering there are differences in several published optical parameters of human head tissues, we further tested if the differences in these optical parameters used in the simulation could lead to significant bias in the result. For this, we performed a simulation using the other optical parameters [19]: the absorbing coefficient μ_a = 0.019, 0.004, 0.02, 0.08 mm^{-1} and the reduced scattering coefficient $\mu_s^{'}$ = 0.858, 0.00099, 0.99, 6.544 mm^{-1} for the skin and skull, cerebral spinal fluid, gray matter and white matter, respectively. The simulation results showed similar optimal combinations of time gates, such as gate opening time and gate width, but the magnitude of the SNR value is different.

In a TD system with a pulsed laser source, due to the fact that the upper limit of the coherence length L_C is governed by the uncertainty principle, and the FWHM of an IRF must be wider than the width of the laser pulse, the coherence length $L_c < 2\ln(2)\frac{4c}{n} \times FWHM$ (for Gaussian emission spectrum), where c is the speed of light, n is the refractive index of the medium. To further investigate how the FWHM and L_C affect the contrast of g_2 between the two brain functional states (i.e., baseline and activation) in the photon noise-free condition, we used simulation methods to calculate the maximal difference of g_2 between the two brain functional states for several IRFs with different FWHMs and corresponding possible L_C. For simplicity, we took Gaussian function as IRF with FWHM from 100 to 400 ps in increments of 50 ps. For each IRF, we estimated the upper limit of the L_C and selected several possible L_C, e.g., from 1.0 cm to the upper limit with a 1.0 cm increment. The gate opening time was from 200 to 1200 ps (relative to the peak time of the IRF), and gate width was from 200-2000 ps. Fig. 6 shows the maximal contrast of g_2 between the baseline and activation conditions for different FWHM and L_C. For each FWHM, the longer the selected L_C, the greater the contrast that can be achieved. Considering the FWHM comes from the pulse width of the source laser and the jitter time of photon detection device, if the FWHM is fixed, choosing a photon detection device with as little jitter time as possible will reduce its contribution to the FWHM, which is beneficial to obtain a long L_C. That is, the FWHM of the IRF is largely dominated by the pulse width of the source laser. Increasing the pulse width may obtain a longer L_C. For a fixed L_C, the narrower the FWHM used, the larger the contrast obtained, because the narrow FWHM can effectively avoid the mixture of short paths and long paths, leading to a higher sensitive detection on dynamics interrogated by the longer paths. However, for a narrow FWHM the L_C cannot be too long, as L_C is constrained by FWHM (exactly speaking by the pulse duration). Therefore, there exists some optimal FWHMs for this simulation, e.g., FWHM = 150-200 ps, with which the higher contrast can be achieved (see the pink and yellow line in Fig. 6).

TD-DCS has attracted a lot of attention in the field of optical brain imaging thanks to its potential to sensitively detect deep blood flow. However, the present simulation results (Fig. 4 and 5) indicate that there is still a challenge for this novel technique in the measurement of in-vivo human brain function, since the factors such as the non-ideal IRF, limited L_C and limited incident light power (which in particular leads to high noise levels of g_2) may reduce the contrast between the baseline and activation. The adverse effects of IRF and L_C on the contrast are shown in Fig. 3. To further show the effect of photon noise on g_2, we

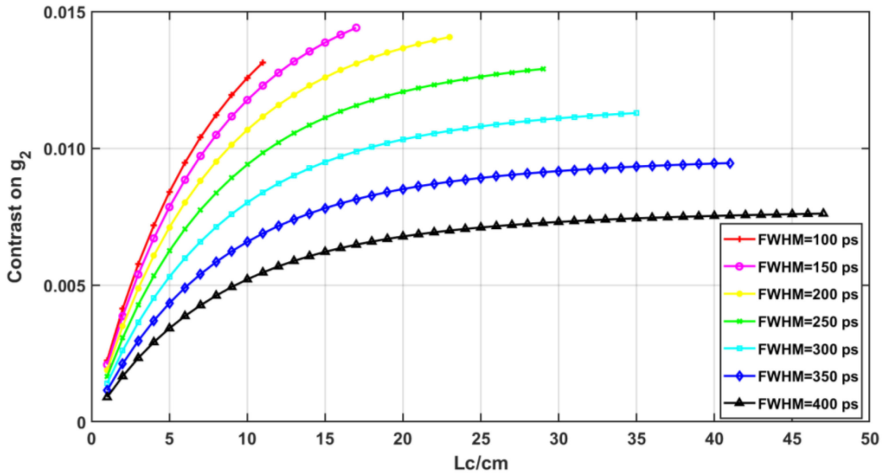

Fig. 6 The maximal contrast on g_2 between the baseline and stimulation in absence of photon noise for a variety of L_C limited by FWHM of IRF.

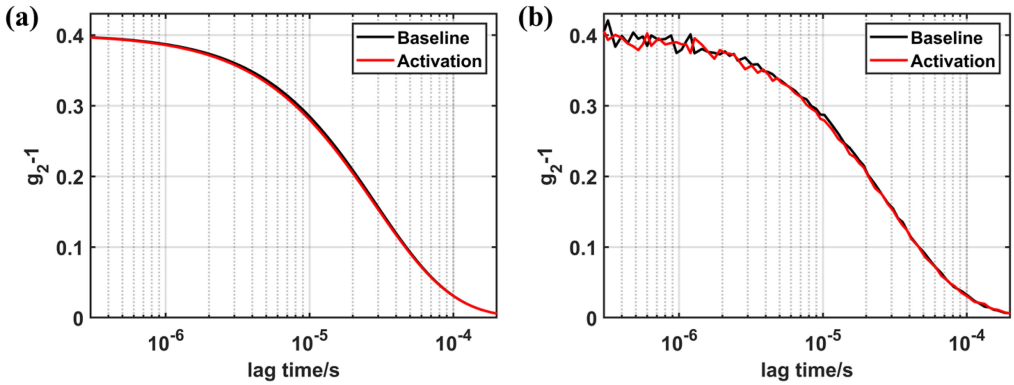

Fig. 7 Simulated photon noise-free g_2 (a) and g_2 with photon noise (b) for the baseline and activation on the conditions of SD = 1.0 cm, input power = 75 mW, L_C = 12 cm, integration time = 10 s, gate opening time t_0 = 800 ps, and gate width T = 1000 ps.

used the optimal parameters (with which the highest SNR values reached) in our simulation, i.e., L_C= 12 cm, integration time = 10 s, t_0= 800 ps and T = 1000 ps, to calculate the simulated g_2 for the baseline and activation condition, as shown in Fig. 7. The noise level was estimated based on Schaetzel model [26]. Even without any photon noise, the difference in g_2 between the baseline and activation was rather small (Fig. 7(a)). For instance, the maximal difference S is 0.0046, which is located at the lag time of 1.1520×10^{-5} s. The noise value N at this lag time is 0.0029, resulting in SNR = 1.580, which is barely to visually see the difference between the baseline and activation (Fig. 7(b)).

It is worth noting that the optimal parameters in this study (e.g., t_0 = 800 ps, T = 1000 ps and L_C = 12 cm) were obtained using simulation methods under the following conditions: illumination power (75 mW), integration time (10 s), SD distance (1.0 cm), a right-tailed IRF (with FWHM of 160 ps), quantum efficiency Q (40%) of photon detector, and the single-mode detector fiber (core diameter Φ = 6.9 um, NA = 0.14). Among these factors, the device-related parameters are IRF, Q, and Φ & NA of single-mode fiber. These parameters have been the best choice (beneficial to the enhancement on the SNR) based on currently available photoelectric elements in order to improve the photon detection efficiency. What we can do to further improve the SNR is to choose the optimal combination of illumination power, integration time, SD distance, gate opening time t_0 and gate width T. However, the maximum illumination power is restricted by the safety limit when detecting human tissues. In order to keep the illumination light intensity below the safe limit (i.e., 4 mW/mm^2) with 75 mW incident power, the illumination spot on the scalp has to be extended to be an area with a radius of 2.44 mm. Higher incident power (e.g., >75 mW) means lower photon noise on g_2, but it also means that a larger illumination area is needed, which is a challenge for measuring the cortical regions on the scalp (except forehead), since hairs will significantly block the light. Therefore, higher illumination power (e.g., higher than 75 mW) is not feasible in measuring human brain. In the measurement of brain function related to hemodynamics, a suitable temporal resolution is needed. Due to the neurovascular coupling, the time scale for a typical hemodynamic response is a couple of seconds, which requires that the temporal resolution of any brain imaging setup used to measure the cerebral hemodynamics should have at least the similar time scale, e.g., a few seconds. The 10 s integration time used in this study is already the upper limit for the brain functional measurement. In other words, further increasing the integration time is not an option, although it is beneficial to

the reduction of photon noise on the measured g_2. Therefore, searching a combination of SD distance, gate opening time and gate width with the goal of maximizing the SNR is a feasible way to optimize TD-DCS measurement on the cerebral blood flow.

In summary, TD-DCS is able to perform path length resolved measurement on the autocorrelation function. In principle, it can achieve sensitive measurement of deep dynamics such as cerebral blood flow by selecting only late arriving photons (late gates). However, the instrument response function and a limited coherence length which are inherent to any TD system significantly reduce the measurement contrast of the changes of cerebral blood flow, which is a challenge for TD-DCS in measuring brain function. Another challenge is the high photon noise in TD-DCS measurements, which is mainly due to the low quantum efficiency of fast photon detector (e.g., $\sim 40\%$ for fast time-resolved detection). The future advance in photon detector with both higher quantum efficiency and fast time-resolution will certainly improve the SNR in TD-DCS measurements. Under the conditions of currently available optoelectronic devices, by optimizing adjustable experimental parameters, the largest SNR value achieved (e.g., 1.580) is marginally able to distinguish the two functional states of the brain: baseline and activation, but it is far from satisfactory in the real application of brain imaging.

V. Conclusion

In this study, we used a MMC to simulate photon propagation in a realistic head model (Collin27). Based on the MMC data, we simulated the time-resolved autocorrelation functions under various conditions, including a typical right-tailed IRF with a FWHM of 160 ps, a limited coherence length of 6 to 12 cm, source-detector spacing of 1.0 cm, incident laser power of 75 mW, the integration time of 5 and 10 s, gate opening time from 200 to 1200 ps (relative to the peak time of the IRF), gate width from 200-2400 ps, and two brain functional states (i.e., baseline and activation). From the simulated autocorrelations, we used SNR to evaluate the change between the baseline and activation for various conditions and found that when the gate opening time is 800 ps and the gate width is equal to or larger than 800 ps, the maximum SNR values can be achieved, indicating that highly sensitive detection of brain functional change can be achieved with these combinations of tunable experimental parameters. This simulation approach and results may be useful for guiding the TD-DCS experiments for measuring human brain function.

Disclosures: The authors of this paper report no relevant financial interests or other potential conflicts of interest to disclose.

References

[1] G. Maret and P. E. Wolf, "Multiple light scattering from disordered media. The effect of brownian motion of scatterers," *Zeitschrift fur Physik B (Condens. Matter),* vol. 65, no. 4, pp. 409–413, 1987.

[2] D. A. Boas and A. G. Yodh, "Spatially varying dynamical properties of turbid media probed with diffusing temporal light correlation," *J. Opt. Soc. Amer. A.,* vol. 14, no. 1, pp. 192–215, 1997.

[3] T. Durduran *et al.*, "Diffuse optical measurement of blood flow in breast tumors," *Opt. Lett.,* vol. 30, no. 21, pp. 2915–2917, 2005.

[4] J. Li *et al.*, "Noninvasive detection of functional brain activity with near-infrared diffusing-wave spectroscopy," *J. Biomed. Opt.,* vol. 10, no. 4, 2005, Art. no. 044002.

[5] G. Yu, T. Durduran, Z. Chao, C. Ran, and A. Yodh, "Near-infrared diffuse correlation spectroscopy for assessment of tissue blood flow," *Handbook of Biomedical Optics*, 1st ed. CRC Press, Boca Raton, FL, USA, 2011, pp. 195–216.

[6] J. Selb, D. A. Boas, S.-T. Chan, K. C. Evans, E. M. Buckley, and S. A. Carp, "Sensitivity of near-infrared spectroscopy and diffuse correlation spectroscopy to brain hemodynamics: Simulations and experimental findings during hypercapnia," *Neurophotonics,* vol. 1, no. 1, 2014, Art. no. 015005.

[7] P. Thong *et al.*, "Early assessment of tumor response to photodynamic therapy using combined diffuse optical and diffuse correlation spectroscopy to predict treatment outcome," *Oncotarget*, vol. 8, no. 12, pp. 19902–19913, 2017.

[8] A. N. S. I. Standard, "Safe use of lasers in health care (electronic version)," *Amer. Nat. Standards Inst. Inc,* vol. Z136.3, 2018, Art. no. 2018.

[9] J. Sutin *et al.*, "Time-domain diffuse correlation spectroscopy," *Optica,* vol. 3, no. 9, pp. 1006–1013, 2016.

[10] A. Pifferi *et al.*, "Time-resolved diffuse reflectance using small source-detector separation and fast single-photon gating," *Phys. Rev. Lett.,* vol. 100, no. 13, 2008, Art. no. 138101.

[11] J. Li, L. Qiu, C.-S. Poon, and U. Sunar, "Analytical models for time-domain diffuse correlation spectroscopy for multi-layer and heterogeneous turbid media," *Biomed. Opt. Exp.,* vol. 8, no. 12, pp. 5518–5532, Dec. 2017.

[12] X. Cheng *et al.*, "Time domain diffuse correlation spectroscopy: Modeling the effects of laser coherence length and instrument response function," *Opt. Lett.,* vol. 43, no. 12, pp. 2756–2759, 2018.

[13] L. Qiu, H. Cheng, A. Torricelli, and J. Li, "Using a simulation approach to optimize time-domain diffuse correlation spectroscopy measurement on human head," *Neurophotonics,* vol. 5, no. 2, 2018, Art. no. 025007.

[14] L. Colombo *et al.*, "Effects of the instrument response function and the gate width in time-domain diffuse correlation spectroscopy: Model and validations," *Neurophotonics,* vol. 6, no. 3, 2019, Art. no. 035001.

[15] M. Pagliazzi *et al.*, "Time domain diffuse correlation spectroscopy with a high coherence pulsed source: In vivo and phantom results," *Biomed. Opt. Exp.,* vol. 8, no. 11, pp. 5311–5325, 2017.

[16] D. Tamborini *et al.*, "Portable system for time-domain diffuse correlation spectroscopy," *IEEE Trans. Biomed. Eng.*, vol. 66, no. 11, pp. 3014–3025, Nov. 2019.

[17] S. Samaei, P. Sawosz, M. Kacprzak, Z. Pastuszak, D. Borycki, and A. Liebert, "Time-domain diffuse correlation spectroscopy (TD-DCS) for noninvasive, depth-dependent blood flow quantification in human tissue in vivo," *Sci. Rep.*, vol. 11, no. 1, pp. 1–10, 2021.

[18] D. J. Pine, D. A. Weitz, J. X. Zhu, and E. Herbolzheimer, "Diffusing-wave spectroscopy: Dynamic light scattering in the multiple scattering limit," *J. de Physique*, vol. 51, no. 18, pp. 2101–2127, 1990.

[19] Q. Fang, "Mesh-based Monte Carlo method using fast ray-tracing in plucker coordinates," *Biomed. Opt. Exp.,* vol. 1, no. 1, pp. 165–175, 2010.

[20] D. L. Collins *et al.*, "Design and construction of a realistic digital brain phantom," *IEEE Trans. Med. Imag.*, vol. 17, no. 3, pp. 463–468, Jun. 1998.

[21] G. Strangman, M. A. Franceschini, and D. A. J. N. Boas, "Factors affecting the accuracy of near-infrared spectroscopy concentration calculations for focal changes in oxygenation parameters," *Neuroimage*, vol. 18, no. 4, pp. 865–879, 2003.

[22] A. Torricelli *et al.*, "Time domain functional NIRS imaging for human brain mapping," *Neuroimage,* vol. 85, pp. 28–50, 2014.

[23] A. Mrwan and M. J. S. Deen, "Time-resolved diffuse optical spectroscopy and imaging using solid-state detectors: Characteristics, present status, and research challenges," *Sensors*, vol. 17, no. 9, 2017, Art. no. 2115.

[24] A. Dalla Mora *et al.*, "Fast-gated single-photon avalanche diode for wide dynamic range near infrared spectroscopy," *IEEE J. Sel. Topics Quant.,* vol. 16, no. 4, pp. 1023–1030, Jul./Aug. 2010.

[25] S. C. Ramsay *et al.*, "Changes in global cerebral blood flow in humans: Effect on regional cerebral blood flow during a neural activation task," *J. Physiol.,* vol. 471, pp. 521–534, 1993.

[26] K. Schatzel, "Noise on photon correlation data. I. Autocorrelation functions," *Quantum Opt.: J. Eur. Opt. Soc. Part B,* vol. 2, no. 4, 1990, Art. no. 287.